


Article

Evaluation of Visual and Nonvisual Levels of Daylight from Spectral Power Distributions Considering Orientation and Seasonality

Silvia Ezpeleta ^{1,2}, Elvira Orduna-Hospital ^{1,2} , Justiniano Aporta ^{1,2}, María José Luesma ^{2,3}, Isabel Pinilla ^{2,4} and Ana Sánchez-Cano ^{1,2,*} 

- ¹ Applied Physics Department, University of Zaragoza, 50009 Zaragoza, Spain; 569761@unizar.es (S.E.); eordunahospital@unizar.es (E.O.-H.); aporta@unizar.es (J.A.)
² Aragon Institute for Health Research (IIS Aragon), 50009 Zaragoza, Spain; mjuesma@unizar.es (M.J.L.); ipinilla@unizar.es (I.P.)
³ Department of Human Anatomy and Histology, University of Zaragoza, 50009 Zaragoza, Spain
⁴ Department of Ophthalmology, Lozano Blesa University Hospital, 50009 Zaragoza, Spain
* Correspondence: anaisa@unizar.es

Abstract: The evaluation of both visual and nonvisual effects from the spectral power distribution (SPD) of outdoor light is critical in lighting design. The dome-light SPD characteristically changes continuously depending on the seasonality, orientation, altitude of the sun or hour of the day. Traditional photopic parameters, such as the illuminance, luminance or correlated colour temperature (CCT), have been widely studied, but presently, there is no melanopic measurement or evaluation method. This article discusses the processes involved in establishing a simple method to determine the SPD of daylight and solar radiation over the skydome in a location to accurately account for the effects of both photopic and circadian levels around a location. Once per month for one year, natural daylight was spectrally measured in the city of Zaragoza (Spain); radiometric and photometric characteristics were analysed by season; and circadian effects were calculated in terms of standard parameters described by the Commission International de l'Eclairage (CIE), factors recommended by normative and scientific backgrounds. Finally, we suggest that the best parameter is the melanopic versus photopic irradiance ratio, which achieves reliable results at simplifying and correlating calculations.

Keywords: daylight; circadian light; spectral power distribution



Citation: Ezpeleta, S.; Orduna-Hospital, E.; Aporta, J.; Luesma, M.J.; Pinilla, I.; Sánchez-Cano, A. Evaluation of Visual and Nonvisual Levels of Daylight from Spectral Power Distributions Considering Orientation and Seasonality. *Appl. Sci.* **2021**, *11*, 5996. <https://doi.org/10.3390/app11135996>

Academic Editor: Tran Quoc Khanh

Received: 21 May 2021
Accepted: 25 June 2021
Published: 28 June 2021

Publisher's Note: MDPI stays neutral with regard to jurisdictional claims in published maps and institutional affiliations.



Copyright: © 2021 by the authors. Licensee MDPI, Basel, Switzerland. This article is an open access article distributed under the terms and conditions of the Creative Commons Attribution (CC BY) license (<https://creativecommons.org/licenses/by/4.0/>).

1. Introduction

The sun is the main source of natural light on Earth; and as natural light passes through the atmosphere, its energy is manifested in the different types of radiation along the electromagnetic spectrum, measured from the ground. The spectral power distribution (SPD) of the light over the skydome is rarely uniform. The amount of visible energy that reaches us depends on the atmosphere. Visible energy can be absorbed, reflected and scattered in all directions by gas and dust particles and clouds of water vapour. The characteristics of the entire sky can change within minutes, so overcast, partly cloudy and clear skies are highly dynamic due to winds. The Commission International de l'Eclairage (CIE) defines the Standard General Skies in the CIE S 011:2003/ISO 15469:2004 [1] as a mathematical model based on the variation in three characteristics: sky clearness and brightness, both derived from a comparison of direct normal and diffuse horizontal irradiance (W/m^2) and/or illuminance (lux); and solar altitude that can be either calculated for a specific date and time or given as a measured angle above the horizontal plane. This model combines five coefficients, which can then be calculated directly from these three values and the position of the sun within the sky, to describe the spatial distribution of 15 diverse sky types; and the luminance for any point on the skydome can be calculated relative to the zenith illuminance [1–3].

The use of irradiance data makes luminance calculations more accurate, as it has been described [4,5]. These general sky types represent a range of different sky conditions from overcast to cloudless with varying levels of direct sunlight. They are approximately illustrative of common sky settings with varying levels of cloudiness and turbidity, and they are commonly used in indoor lighting design software. Knowledge of the irradiance distribution of the sky is essential to achieve a good natural lighting design in indoor areas. It is important to know how the characteristics of the sky change in different periods of the year, depending on the climate of the specific place in which we want to conduct the measurements, the types of clouds, the light distribution, the illuminance, the geographical location, the time, etc. Daylight greatly influences the energy efficiency of a building. Despite the advances in artificial lighting, it is still difficult to reduce the energy consumption of large buildings. According to the Office Energy Saving and Efficiency Guide, 40% of the world's energy consumption is produced by buildings. A good estimate of daylight will help reduce electric light consumption. Using the universal method provided by the CIE, the luminance of the sky and thus daylight can be partially predicted. Currently, both irradiance and illuminance levels, mainly at vertical and inclined planes, from the sky are needed for proper building design [3,5–7], but studies seeking to resolve the problem of finding artificial lighting with similar behaviour to the solar SPD have been partially developed.

The correlated colour temperature (CCT) and the colour rendering index (CRI) are parameters used to visually characterize light and lighting strategies, but light reaching the eye level has two important objectives: first, this light is responsible for forming images; and second, this light is part of the exposome [8], meaning it is essential in the synchronization of the circadian system, the system in charge of setting our biological clock on time each day in accordance with the cycles of day and night (light-dark) [9]. Regulating the amount of light that reaches the corneal level and improving environmental conditions could have positive impacts on quality of life, wellbeing, and ageing-related concerns. These lighting projects, which consider the potential effects of light on people and optimize them to achieve the greatest wellbeing, are called human-centric lighting (HCL) projects. However, the increasing number of such projects does not correspond to the importance that circadian light should have according to relevant indoor studies. A lack of knowledge has revealed how the characteristics of outdoor daylight are considered to perform indoor lighting designs. Beyond visual stimuli, the CIE S 026/E: 2018 standard [10] includes information concerning the effects of light on intrinsically photoreceptive retinal ganglion cells (ipRGCs) that are related to the SPD, temporal distribution or photoperiod: dynamic light, which is the right light at the right time [11,12]. Even the International WELL Building Standard (Visual lighting design and Circadian lighting design) recommends lighting guidelines to provide appropriate photopic and scotopic light levels, minimize disruption to the body's circadian system, and support good sleep quality [13]. Currently, lighting projects consider that the circadian rhythm in humans is described as an approximately 24 h cycle controlled by the lighting environment and one of the keys to regulating sleep, mood, heart rate and body temperature [14]. Nowadays, people stay indoors with artificial lighting and with relatively limited sunlight most of their time awake, or under the influence of secondary sources such as screens; these environmental contributions should be globally evaluated in circadian terms [15]. The CIE divides the visual from nonvisual effects of light and is developing integrative standards from this perspective [10]. To fulfil this objective, special attention has to be paid to the SPD. Both the excitation of traditional photoreceptors and ipRGCs are highly wavelength-dependent and form two interdependent pathways for light in the brain [16]. To evaluate and quantify the visual and nonvisual influences of light in humans belonging anatomically to these two ocular pathways, the CIE adopted the proposal of Lucas et al. defining that the influences are physically characterized by five equivalent α -opic illuminance approaches. This standard employs light measurement methods that quantify the effective irradiance for each of the photoreceptive inputs to the visual system independently. The CIE S 026/E:2018 [10] adopted melanopic equivalent daylight (D_{65}) illuminance, which the Equivalent Daylight Illuminance (EDI) defined as a

light source-type D₆₅ that employs photopic illuminance $E_{\text{photopic,D65}}$ to provide the same melanopic irradiance as a light source with the SPD and photopic illuminance $E_{\text{photopic,SPD}}$. An important issue found for accurate visual and nonvisual daylight implications is the limited information available for this analysis because at least six factors triggering nonvisual light effects have been summarized, including the SPD, the irradiance level, the directionality, the timing, the duration, and the history, which are grouped into luminous and temporal categories [11]. Nevertheless, there have been efforts to develop a clear method to evaluate the effects of lighting on circadian rhythm regulation from different perspectives [17,18].

This research hypothesizes that daylighting SPDs modify the photopic and melanopic levels inside buildings depending on the orientation, seasonality and characteristics of the skydome [17,18]. The aim of this study is to analyse these real seasonal changes in natural sunlight to evaluate how changes in the SPD affect photometric quantities and calculate the variations in circadian magnitudes based on the CIE standard. Knowledge of the outdoor daylight is essential to achieve a good natural lighting design in indoor areas from a wellbeing perspective. Differences in daylight with geographical location of a building, façade orientations or seasonality should be analyzed and considered to evaluate the nonvisual potential of daylight for indoor lighting purposes. This analysis leads us to evaluate the main parameters that should be considered by indoor designers to simulate daylight conditions with artificial lighting promoting people's wellbeing.

2. Materials and Methods

2.1. Spectral Measurements

The methodology of this research was based on the analysis of the radiometric behaviour of the daylight at a location, which serves to model their circadian contribution at this same point. We conducted several spectral measurements of the skydome over one year from December 2018 to November 2019. We sought a sunny day around the 15th of each month, and measurements were performed from 10:00 to 11:00 a.m. The experiment was located at the roof of the Sciences Faculty at the University of Zaragoza in Spain (41°38'31" N, 0°53'60" W; 243 m above sea level). The SPD measurements were performed with a calibrated spectroradiometer (Avaspec-1024, Avantes, Apeldoorn, The Netherlands, NPL E01110063/DDK calibration and NIST traceability). A tripod was used to ensure accurate measurements of the spectra in the four cardinal directions (north, south, east and west) 15°, 30°, and 45° from the horizontal plane. To register information about the weather, photos of the sky were taken. The sky conditions were always clear except intermediate skies with visible sun and a few clouds.

2.2. Theoretical Considerations

The SPD ($\mu\text{W}/\text{cm}^2$) from 300 nm to 1000 nm, the CCT, and the colour coordinates x and y of the selected day were recorded for further processing. The photopic irradiance $E_{e,\text{photopic}}$ (W/m^2) = $\int_{\lambda=380}^{780} \text{SPD}(\lambda)V(\lambda)d\lambda$ and illuminance E_{photopic} (lux) = $K_m \int_{\lambda=380}^{780} \text{SPD}(\lambda)V(\lambda)d\lambda$, were determined ($K_m = \frac{683\text{lm}}{\text{W}}$ for photopic vision, $\text{SPD}(\lambda)$ is the spectral power distribution of the lighting source and $V(\lambda)$ is the CIE photopic spectral luminous efficiency function) [10,19]. The melanopic irradiance $E_{e,\text{melanopic}}$ (W/m^2) = $\int_{\lambda=380}^{780} \text{SPD}(\lambda)S_{\text{mel}}(\lambda)d\lambda$ was analogously calculated ($S_{\text{mel}}(\lambda)$ is the CIE melanopic spectral weighting function) [10]. The ratio $\frac{E_{e,\text{melanopic}}}{E_{e,\text{photopic}}}$ is named the Melanopic Action Factor (MAF) [20], following the Circadian Action Factor (CAF) proposed by Gall [21], based on spectral irradiance behaviour and was used to propose a method to evaluate the nonvisual potential of daylight. In a previous publication by this research group, the conversion factors from photopic values of illuminance to the CIE melanopic standard and to other recommendations such as WELL were calculated in detail [20]. To understand these conversions, a summary of the equations is added.

The normalization imposed by the CIE standard with melanopic illuminance was provided by the standard illuminant D_{65} (daylight CCT = 6500 K) in accordance with the EDI. A light-source type D_{65} furnishing photopic illuminance $E_{e,photopic,D65}$ to provide the same melanopic illuminance $E_{melanopic,D65}$ can be calculated.

If the photometric quantity is defined by $E_{photopic,D65} = K_m E_{e,photopic,D65}$ [19], the same melanopic $E_{melanopic,D65} = K_{melanopic,D65} E_{e,photopic,D65}$ for light source D_{65} can be described in terms of an equality as follows: $E_{photopic,D65} = E_{melanopic,D65}$. For any source:

$$EDI = 753.8 \int_{\lambda=380}^{780} SPD(\lambda) S_{mel}(\lambda) d\lambda$$

In addition, the relation of the EDI with the photometric illuminance can be deduced as follows [20]:

$$EDI = 1.104 \text{ MAF } E_{photopic}$$

The Equivalent Melanopic Lux (EML) is defined by the WELL recommendations [13] with reference to the equi-energy illuminance and can be calculated for any source, in terms of melanopic parameters; the EML is defined as follows [20]:

$$EML = 831.8 \int_{\lambda=380}^{780} SPD(\lambda) S_{mel}(\lambda) d\lambda$$

In addition, the relation of the EML to photometric illuminance is described as follows:

$$EML = 1.218 \text{ MAF } E_{photopic}$$

Using these conversion factors and photopic values of the illuminance, transformations from one melanopic metric to another are easily calculated by $EML = 1.104 \text{ EDI}$.

3. Results and Discussion

Outdoor SPD measurements in Zaragoza, Spain (latitude: 41.6370082° , longitude: -0.9078846°) are provided facing the four main cardinal points (north, east, south and west) 15° , 30° , and 45° from the horizontal plane. The seasonal irradiance ($\mu\text{W}/\text{cm}^2$) from 380 to 780 nm, luminance (cd/m^2), illuminance (lux), and CCT (K) were calculated from the SPD measurements to estimate variations depending on altitude and orientation. Calculations of nonvisual effects using the previously described metrics were performed to analyse values, compare current melanopic evaluation methods and estimate the variability ranges of daylight.

3.1. Sky Characteristics and Photopic Descriptions

The outdoor solar conditions of the study during the experiment were registered (Table 1), and the SPDs were measured (Figure 1).

The highest irradiances can be found in the east direction at 30° – 45° in practically every month except in December, January and October. In those three months, at 15° , the irradiance is higher than that at 45° . This is followed by the south direction, except in January and November. In those two months, at 15° , the irradiance is higher than at 45° . The lowest irradiances are in the west orientation except in five months (February, March, September, October and November), which slightly exceed the values in the north direction (Table 1 and Figure 2). From April to September, the sun is located in the east and at the highest latitudes (Table 1 and Figure 2). In the normalized SPD curves (Figure 1), spectral variations were found throughout the months of the year and depended on the cardinal points at which the measurements were taken.

Table 1. Irradiance E_e ($\mu\text{W}/\text{cm}^2$) and luminance L (cd/m^2) depending on the orientation (north, east, south, and west), elevation (15° , 30° , and 45°) and seasonality.



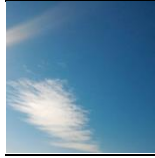




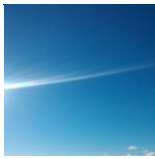
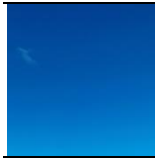

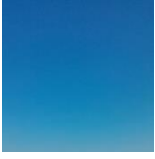












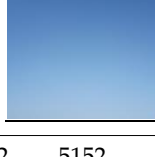

	NORTH			EAST			SOUTH			WEST		
	15°	30°	45°	15°	30°	45°	15°	30°	45°	15°	30°	45°
12 December 2018												
E_e ($\mu\text{W}/\text{cm}^2$)	3197	3047	2839	19,081	19,436	17,576	35,271	36,212	35,274	2894	2899	2918
L (cd/m^2)	444	3574	2240	4787	4059	2628	18,590	12,960	15,220	3319	2592	1643
21 January 2019												
E_e ($\mu\text{W}/\text{cm}^2$)	3340	3134	2830	25,475	25,922	25,277	29,394	29,973	27,607	2987	2943	2724
L (cd/m^2)	5017	2596	1703	4983	3708	2475	9360	6400	3922	3851	2898	1423
21 February 2019												
E_e ($\mu\text{W}/\text{cm}^2$)	3931	3896	4077	28,019	30,388	30,585	28,827	31,191	31,232	4348	4100	4465
L (cd/m^2)	3045	2064	1820	11,020	8730	5019	8430	5521	4837	2600	1696	1401
18 March 2019												
E_e ($\mu\text{W}/\text{cm}^2$)	3191	2878	2588	38,413	41,519	39,197	24,936	29,386	32,138	3802	3490	3139
L (cd/m^2)	2200	1322	1016	4055	2706	2368	3955	2500	2176	2800	1390	1062
12 April 2019												
E_e ($\mu\text{W}/\text{cm}^2$)	4885	5283	8752	37,091	38,974	37,395	11,822	15,363	18,544	4132	5152	4420
L (cd/m^2)	3333	3290	2942	17,990	19,330	18,840	5930	6211	18,840	3450	3317	1076

Table 1. Cont.

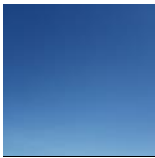
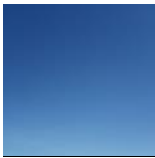
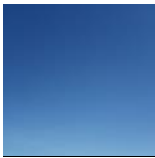
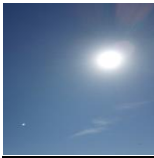
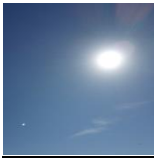
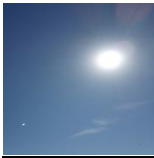
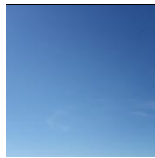
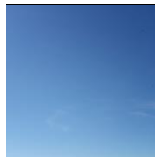
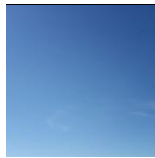
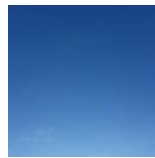
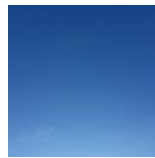
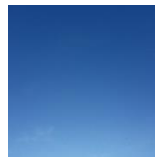
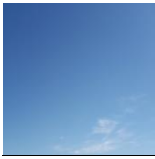
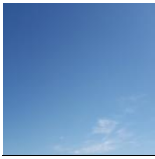
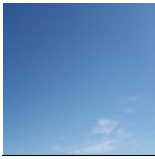
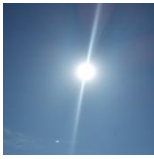
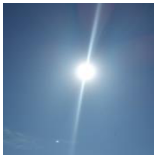
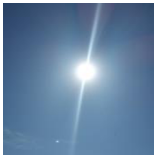
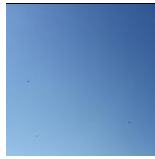
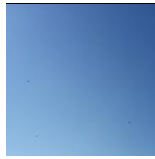
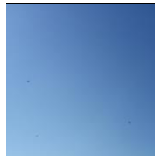
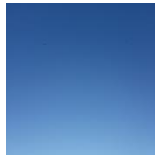
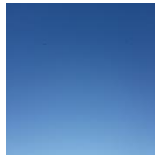
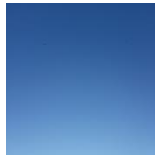



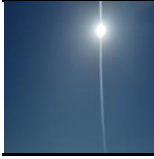
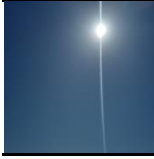
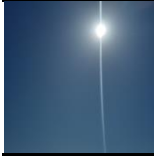
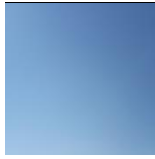
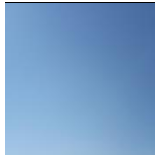
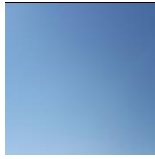
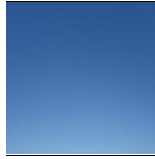
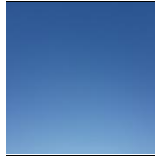
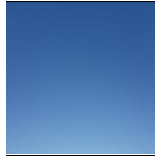
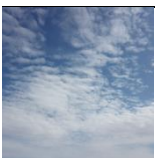
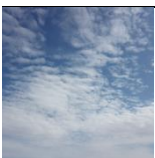
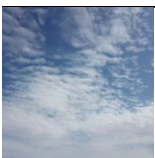
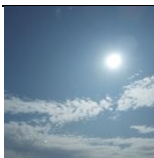
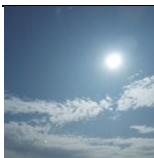
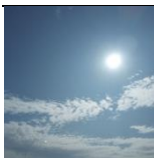
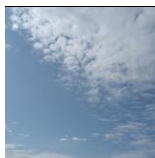
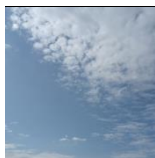
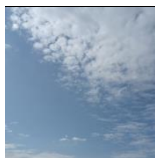
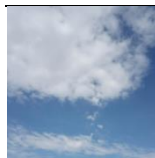
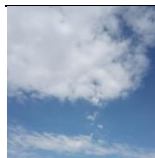
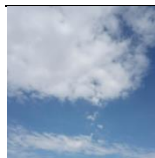






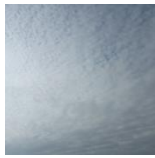
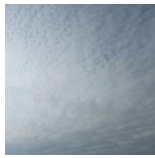
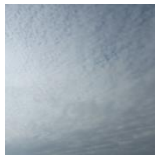






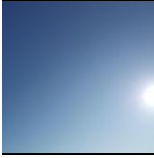
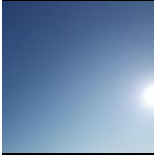
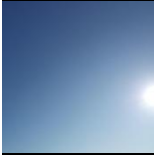



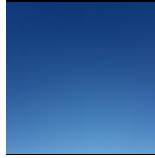
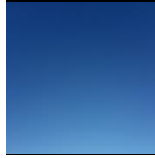
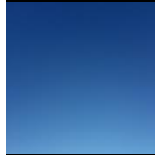
	NORTH			EAST			SOUTH			WEST		
	15°	30°	45°	15°	30°	45°	15°	30°	45°	15°	30°	45°
14 May 2019												
E_e ($\mu\text{W}/\text{cm}^2$)	4780	9791	15,429	40,761	44,519	44,569	7907	14,418	20,406	3748	3488	3128
L (cd/m^2)	3419	1791	1224	7720	5098	5996	4020	2287	1775	2384	1919	1138
17 June 2019												
E_e ($\mu\text{W}/\text{cm}^2$)	8067	13,439	17,755	39,660	43,915	45,014	4798	18,450	23,816	4131	3792	3659
L (cd/m^2)	3883	2339	1742	10,310	8200	9410	4430	2567	2046	4179	2300	1399
12 July 2019												
E_e ($\mu\text{W}/\text{cm}^2$)	4897	11,880	18,786	34,359	39,698	42,941	18,469	25,596	31,130	4666	4240	4260
L (cd/m^2)	20,000	12,340	8820	41,100	29,450	29,150	29,090	16,230	13,120	19,420	11,030	7160
13 August 2019												
E_e ($\mu\text{W}/\text{cm}^2$)	7624	11,232	17,794	42,764	46,853	47,244	13,897	20,120	24,896	6794	7255	8033
L (cd/m^2)	7293	7891	6885	14,830	7891	6885	10,040	8193	5290	2598	4290	6031
16 September 2019												
E_e ($\mu\text{W}/\text{cm}^2$)	5060	5512	6596	33,242	34,991	34,059	16,551	20,065	22,074	5460	5851	6522
L (cd/m^2)	3641	2839	3239	16,270	18,250	23,760	4598	6454	9320	3939	4461	5169
15 October 2019												
E_e ($\mu\text{W}/\text{cm}^2$)	3092	2923	2734	35,241	35,516	33,065	21,147	22,845	24,149	3201	2989	2714
L (cd/m^2)	2802	1461	908	6716	5142	2509	4388	2507	1625	3594	1762	1022

Table 1. Cont.

	NORTH			EAST			SOUTH			WEST		
	15°	30°	45°	15°	30°	45°	15°	30°	45°	15°	30°	45°
13 November 2019												
E_e ($\mu\text{W}/\text{cm}^2$)	3877	4593	4224	44,067	46,117	45,410	28,262	26,410	21,544	4503	4915	4786
L (cd/m^2)	2253	1636	1050	6147	2931	1823	9380	5776	4424	3405	1758	1167

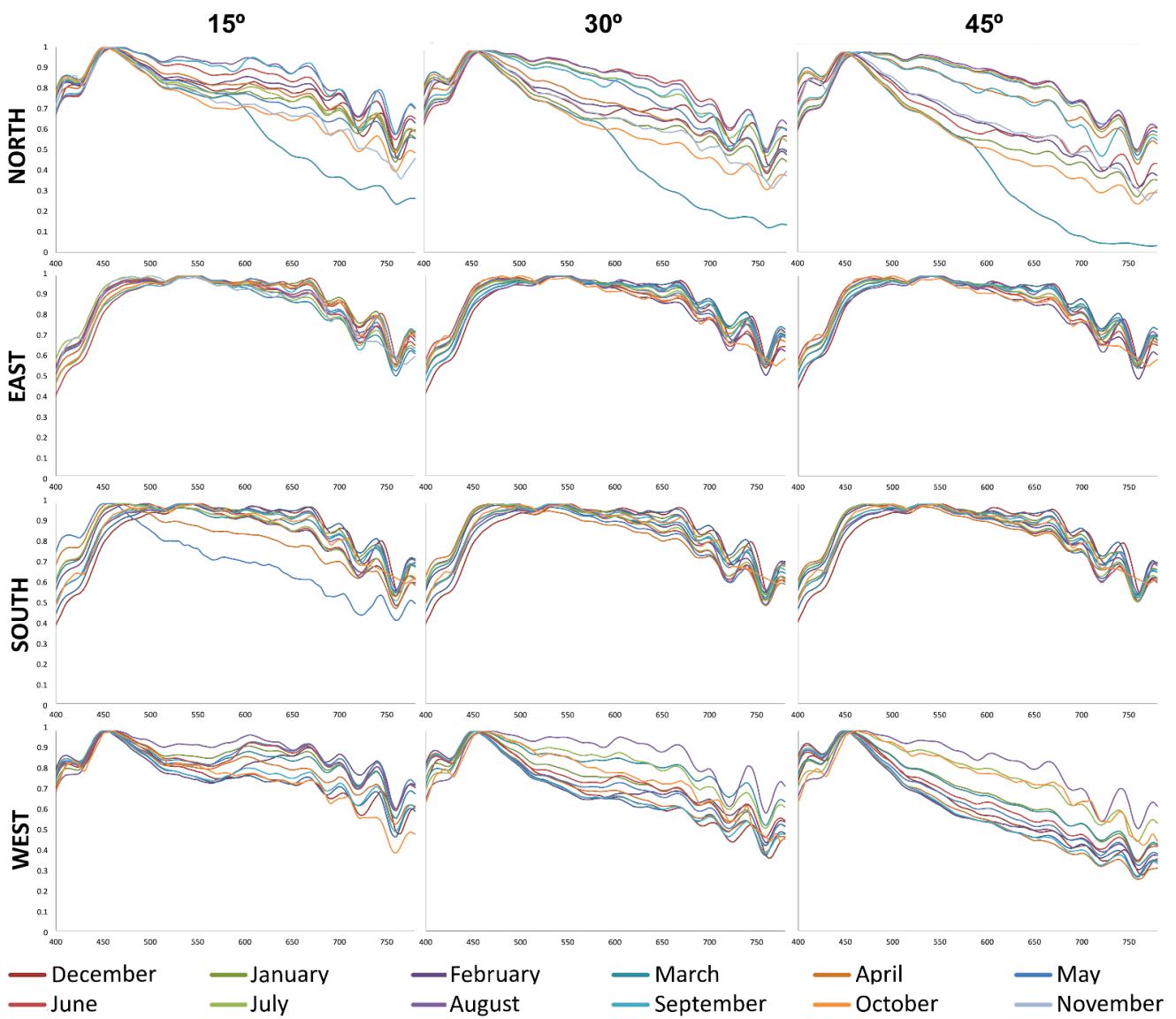


Figure 1. Normalized spectral power distribution depending on the orientation (north, east, south, and west), elevation (15°, 30°, and 45°) and seasonality.

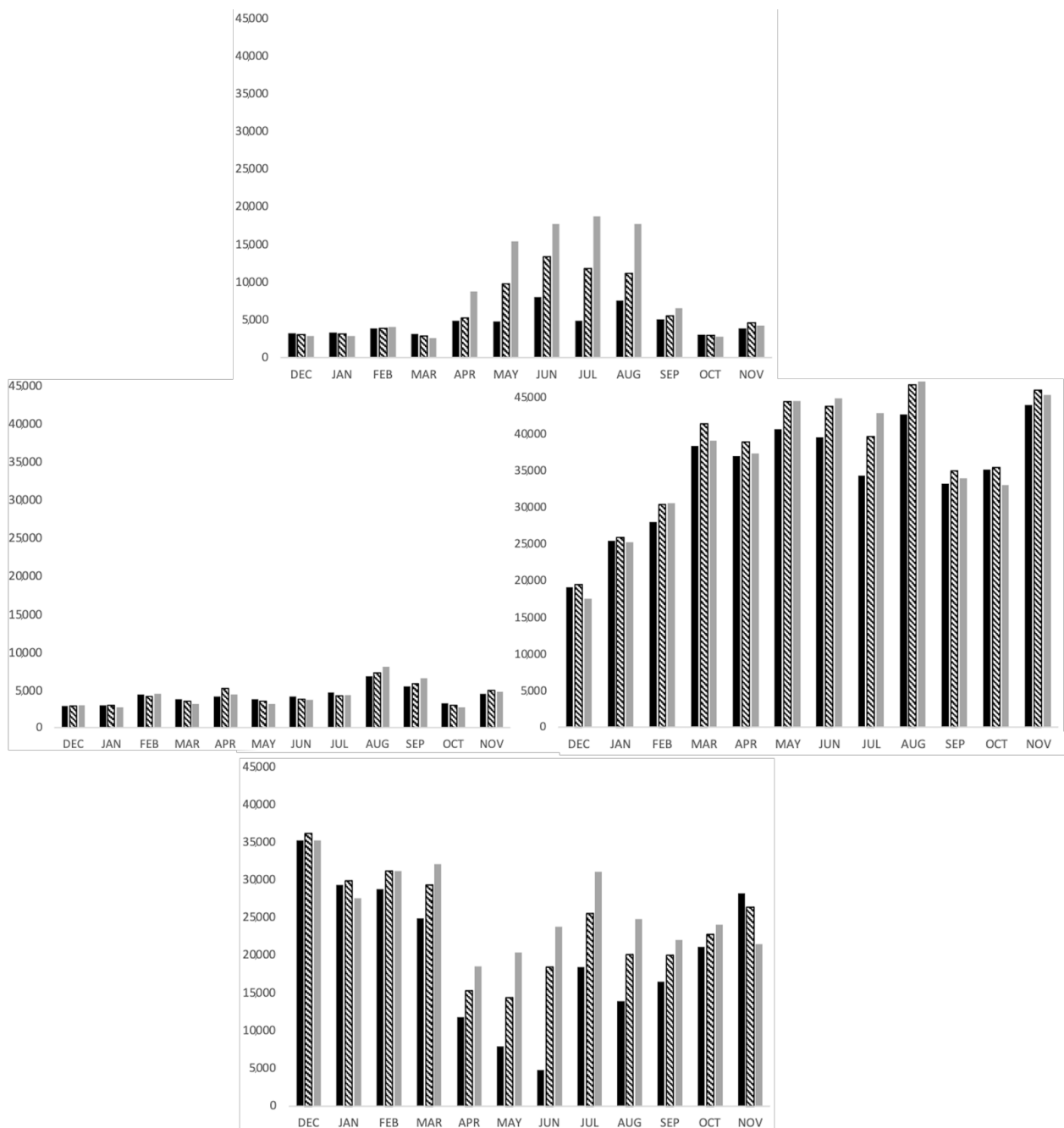


Figure 2. Irradiances from 380 to 780 nm ($\mu\text{W}/\text{cm}^2$) measured depending on the season (from December 2018 to November 2019); orientation of north (**top**), east (**right**), south (**bottom**), and west (**left**); and elevation from the horizontal level of 15° (black), 30° (striped), and 45° (grey).

In most of the data, higher CCTs were found in the north and west orientations than in the east and south orientations and in the winter months (from December to March) and some of the autumn months, especially in October (Figure 3). In general, the CCTs are higher in measurements taken at 45° and lower in those taken at 15° . The average CCT was 6122 K; the maximum value was taken in March, facing north at 45° (12,380 K); and the minimum was taken in December, facing south at 15° (4892 K). In general, the CCTs where the sun is located (south and east) always comprised warmer restricted ranges irrespective of the season and the sky altitude. Conversely, in the opposite locations (north and west), the CCTs are altitude-dependent; and the higher the CCT is, the cooler the results that are

found. The measured CCTs show variations as a function of the season, orientation and altitude in correspondence with CIE D illuminances, even with clear sky conditions [22,23].

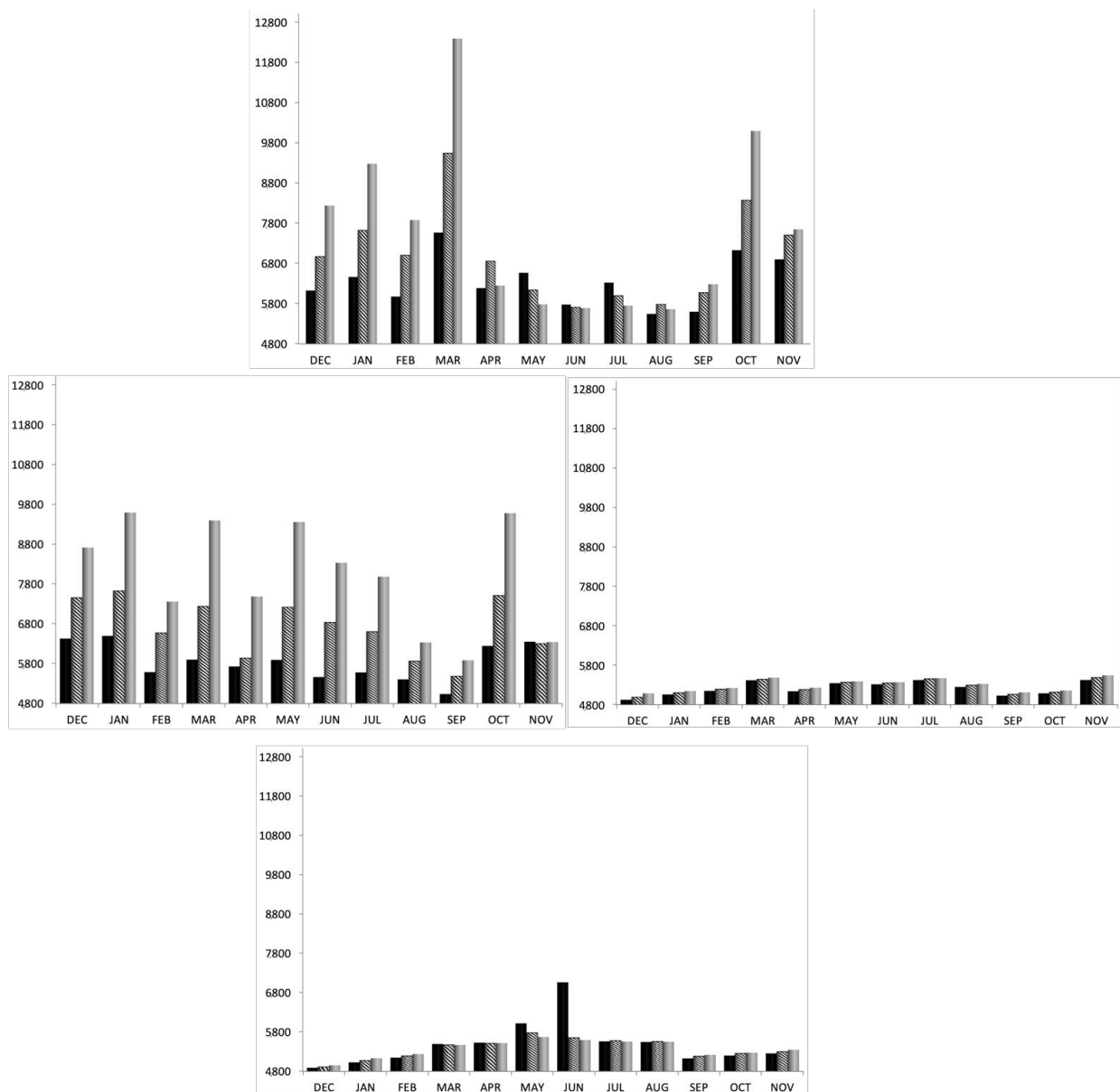


Figure 3. CCT (K) measured depending on the season (from December 2018 to November 2019); orientation of north (top), east (right), south (down), and west (left); and elevation from the horizontal level of 15° (black), 30° (striped), and 45° (grey).

When the value of the sky is considered, daylight approaches 6500 K. The average value of the data taken in this study is 6122 K, similar to the dominant CCT of the study conducted in the city of Granada, Spain (5700 K). However, the recorded data show there were variations throughout the year, which highlights the importance of studying the parameters of the daylight in each type of sky and in different climatic conditions [24]. Although the CCT measurement gives us information mainly on the appearance of colour and on aesthetic perception, its influence on circadian effects can also be considered.

Our experiment was performed in an urban environment, and it did not consider either the level or the components of the atmosphere. The presence of aerosol particles at certain times of the year could influence the presented SPD measures and, consequently, the subsequent calculations [25]. Peyvandi et al. [26] calculated the 25% and 75% interquartile values of the CCT to find the range containing 50% of the CCTs for each condition, obtaining

a range for clear sky without aerosol particles of 5889–6294 K, a range for clear sky with aerosol particles of 5712–6325 K, and a range for overcast sky of 6218–7757 K. The overcast sky and atmosphere with aerosol particles represented extreme conditions where the limits of the CCT were observed. Daylight measured in Granada (Spain), with the most observed CCTs of 5555–5715 K [24], and in Boulder, Colorado (United States), with obtained CCTs of 5500–6400 K, showed that lower CCTs represented atmospheres with higher aerosol particle levels [23,24]. Similar results were found in Rochester, New York (United States), where daylight with CCT as low as 3530 K in a hazy sky was reported [27]. In Zaragoza, the mean CCTs obtained at 45° were 7574 K to the north (range 5660–12,380 K), 5377 K to the south (range 4954–5671 K), 5294 K to the east (range 5085–5543 K), and 8025 K to the west (range 5883–9587 K), irrespective of the presence of clouds, mainly due to the season and showing a broad range of daylight CCTs. Comparing our results with those previous results show very low rates of aerosol elements during all the seasons of the evaluated year.

Luminance patterns of the 15 CIE standard skies have been described and used together with several skydome parameters including different illuminance levels or vertical sky components to classify daylight [1]. Sky luminance values have a strong dependence on its particular conditions such as clouds, which can vary in minutes; or the locations of measurement points that can have different conditions, even when they are nearby [28]. Therefore, the same categories of sky conditions, including clear sky, partly cloudy and overcast, cannot be considered to have similar luminance levels. We chose similar clear skies to perform our experiment, but the location of the sun, partially cloudy skies, and even the buildings of the surroundings highly influenced the results. At 15°, values elevated enough to be considered to have been influenced by the buildings located around the measurement station can be observed (Figure 4). Despite this result, the highest luminance values were found at 45° at the nearby positions where the sun was placed during the measurements. Clouds influenced the measurements, as reflected in the September data, due to the presence of some clouds during the measurement (Table 1).

Higher levels of photopic illuminance (Figure 5) are reached in the east orientation from March to August and in the south direction from September to March compared to the north and west orientations. The months with the highest photopic illuminance are generally in the summer months and in part of the spring months (from May to August), decreasing in the autumn and winter months in the east at the three elevations (15°, 30° and 45°). However, in the south orientation, many differences in photopic illuminance are seen between the three elevations in the spring and summer months (from April to August), which become equal in the autumn and winter months (from September to March). These differences in the three elevations in spring and summer also occur in the north (from May to August). This does not happen in the west orientation, where the photopic illuminance at the three elevations is very equal during all months of the year. The minimum photopic illuminance was found in the month of January in the west orientation with an angle of 45° (5084 lux). The maximum value was found in the month of August in the east orientation with an angle of 45° (99,822 lux). In general, the lowest photopic illuminances were obtained for measurements taken at 15°, and the highest values were obtained for measurements taken at 45°. Illuminance measurements reveal the changing position of the sun with seasons. Regarding the measurement locations, Figures 1 and 5 show that the illuminance level reached higher values while it was positioned 45° in the southeast during autumn–winter and northeast in spring–summer.

3.2. Circadian Characteristics

To assess the circadian characteristics, we began by analysing the parameter MAF (Table 2).

The highest MAFs occur in the north and in the west with a 45° elevation from October to March. Specifically, the highest MAF is 1.156, which is located in the north in March at 45°. The most uniform MAFs occur in the east during all months of the year and at the three elevations. The lowest MAF is 0.759, located in the south in December at 15°.

The mean MAF of all calculated values for the north, south, east and west and for the three elevations (mean ± standard deviation) is 0.871 ± 0.089 with an annual variation of less than 10%. That is, the MAFs are very close to 1, which means that the evaluated daylight has almost equal photopic and melanopic intensities, which will generate the same image-forming and non-image-forming effects.

According to the CIE calculations, higher levels of melanopic EDI are reached (Figure 6) in the east and south orientations compared to the north and west orientations. The months with the highest EDIs were generally the summer months, and the minimum EDI was found in December facing west at an angle of 15° (5656 melanopic lux). The maximum value was taken in August in an east orientation with an angle of 45° (88,714 melanopic lux). In general, the lowest melanopic illuminances have been obtained in measurements taken at 15° , and the highest values have been obtained in measurements taken at 45° .

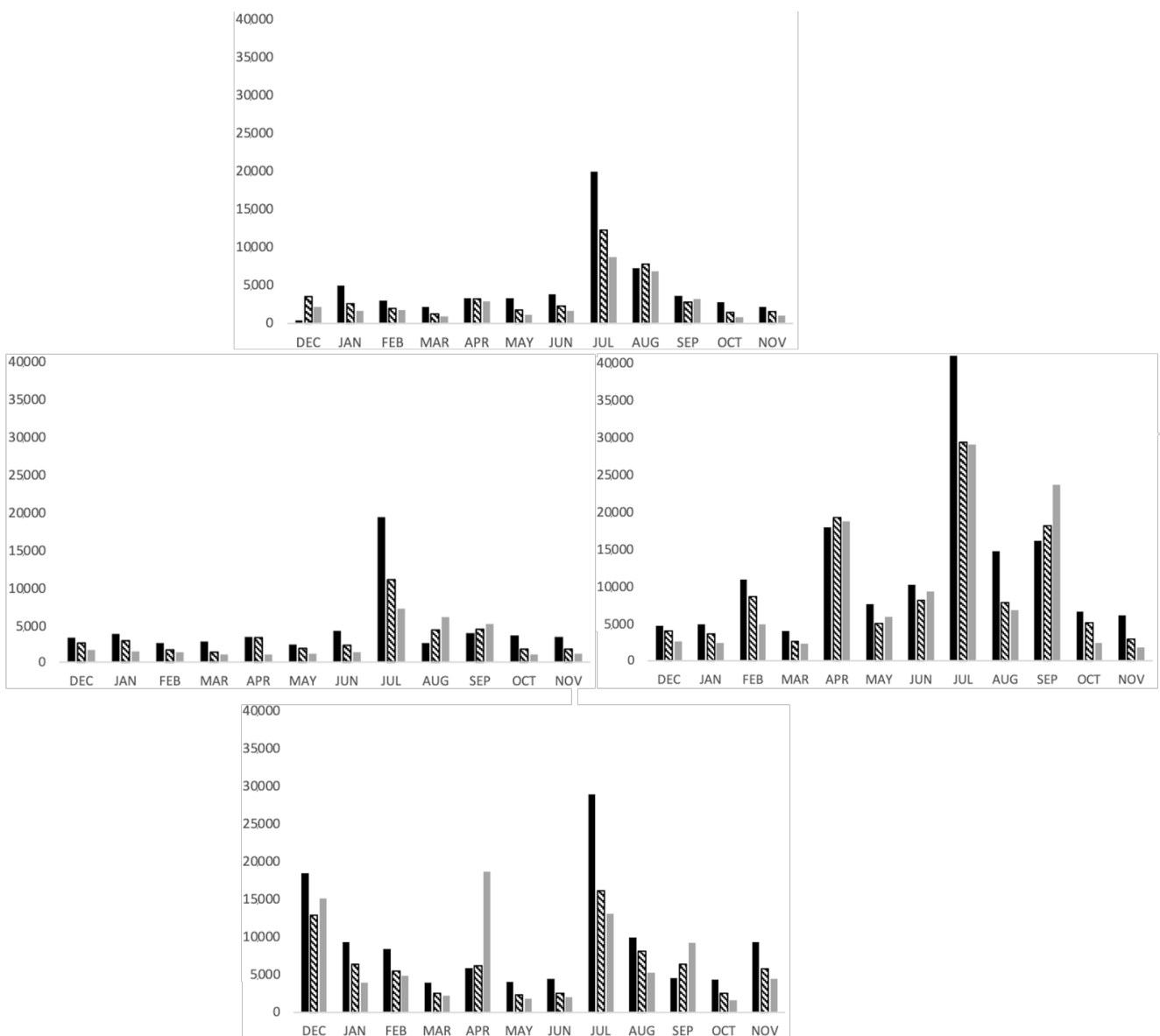


Figure 4. Luminance (cd/m^2) values measured depending on the season (from December 2018 to November 2019); orientation of north (**top**), east (**right**), south (**down**), and west (**left**); and elevation from the horizontal level of 15° (black), 30° (striped), and 45° (grey).

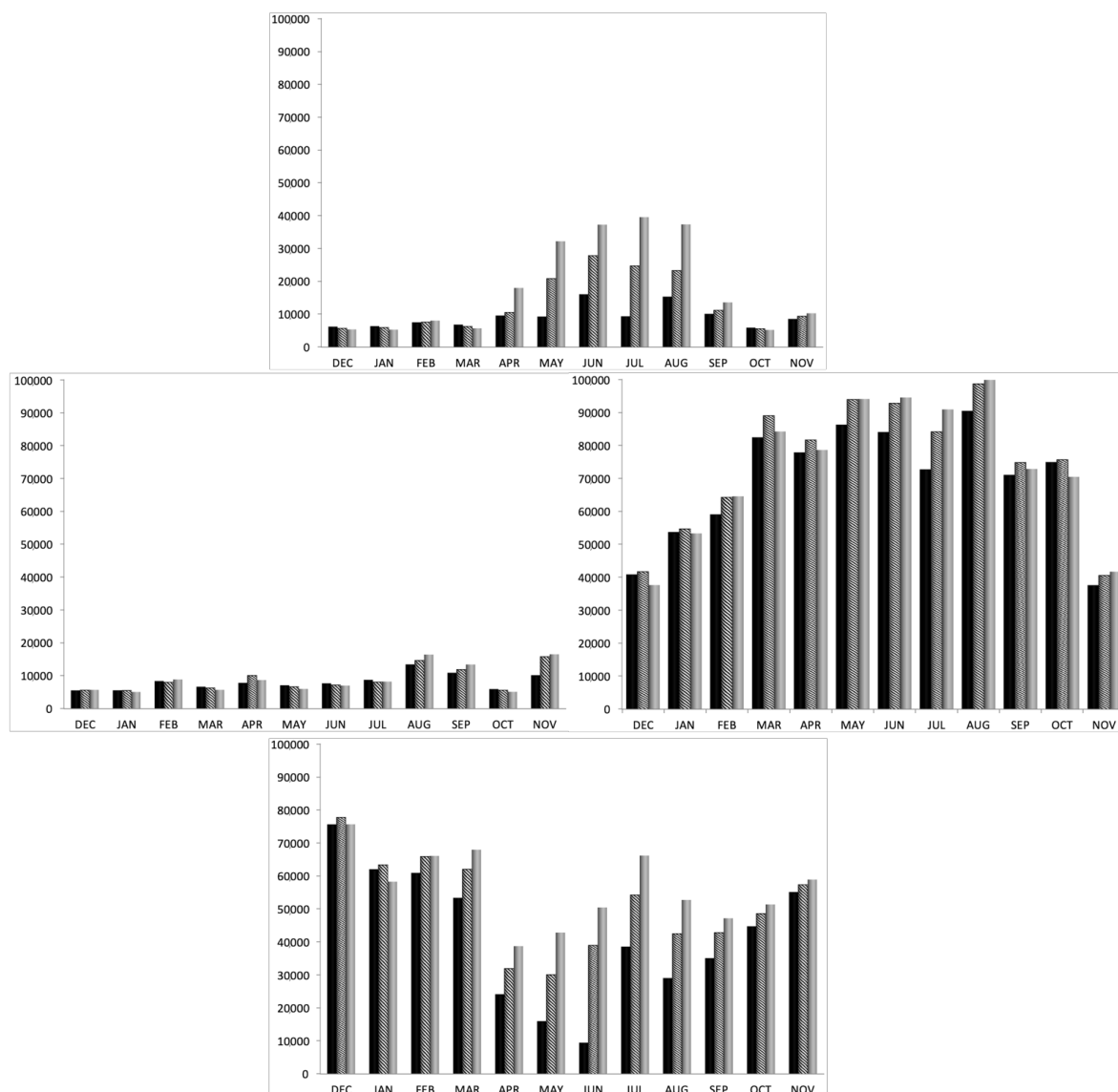


Figure 5. Photopic illuminance (lux) values measured depending on the season (from December 2018 to November 2019); orientation of north (top), east (right), south (down), and west (left); and elevation from the horizontal level of 15° (black), 30° (striped), and 45° (grey).

Table 2. Melanopic Action Factor (MAF) values calculated depending on the season (from December 2018 to November 2019); orientation of north, east, south, and west; and elevation from the horizontal level of 15°, 30°, and 45°.

MAF	NORTH			SOUTH			EAST			WEST		
	15°	30°	45°	15°	30°	45°	15°	30°	45°	15°	30°	45°
DEC	0.900	0.966	1.034	0.759	0.760	0.760	0.763	0.770	0.781	0.923	0.988	1.052
JAN	0.923	0.998	1.079	0.777	0.781	0.788	0.780	0.785	0.789	0.928	0.996	1.089
FEB	0.884	0.953	1.002	0.788	0.793	0.797	0.788	0.792	0.796	0.885	0.924	0.972
MAR	0.964	1.058	1.156	0.821	0.821	0.819	0.811	0.813	0.816	0.901	0.983	1.081
APR	0.897	0.941	0.892	0.834	0.828	0.827	0.789	0.793	0.770	0.867	0.876	0.980
MAY	0.923	0.877	0.850	0.879	0.852	0.839	0.807	0.808	0.811	0.879	0.969	1.069
JUN	0.865	0.848	0.841	0.958	0.838	0.831	0.805	0.808	0.809	0.852	0.947	1.026
JUL	0.911	0.868	0.845	0.832	0.830	0.827	0.815	0.817	0.818	0.856	0.933	1.009
AUG	0.837	0.851	0.838	0.831	0.829	0.827	0.798	0.802	0.805	0.829	0.864	0.897
SEP	0.845	0.881	0.894	0.786	0.789	0.792	0.772	0.775	0.780	0.790	0.829	0.861
OCT	0.966	1.033	1.105	0.795	0.799	0.801	0.781	0.783	0.788	0.914	0.990	1.085
NOV	0.952	0.986	0.993	0.801	0.805	0.810	0.819	0.825	0.830	0.912	0.902	0.904

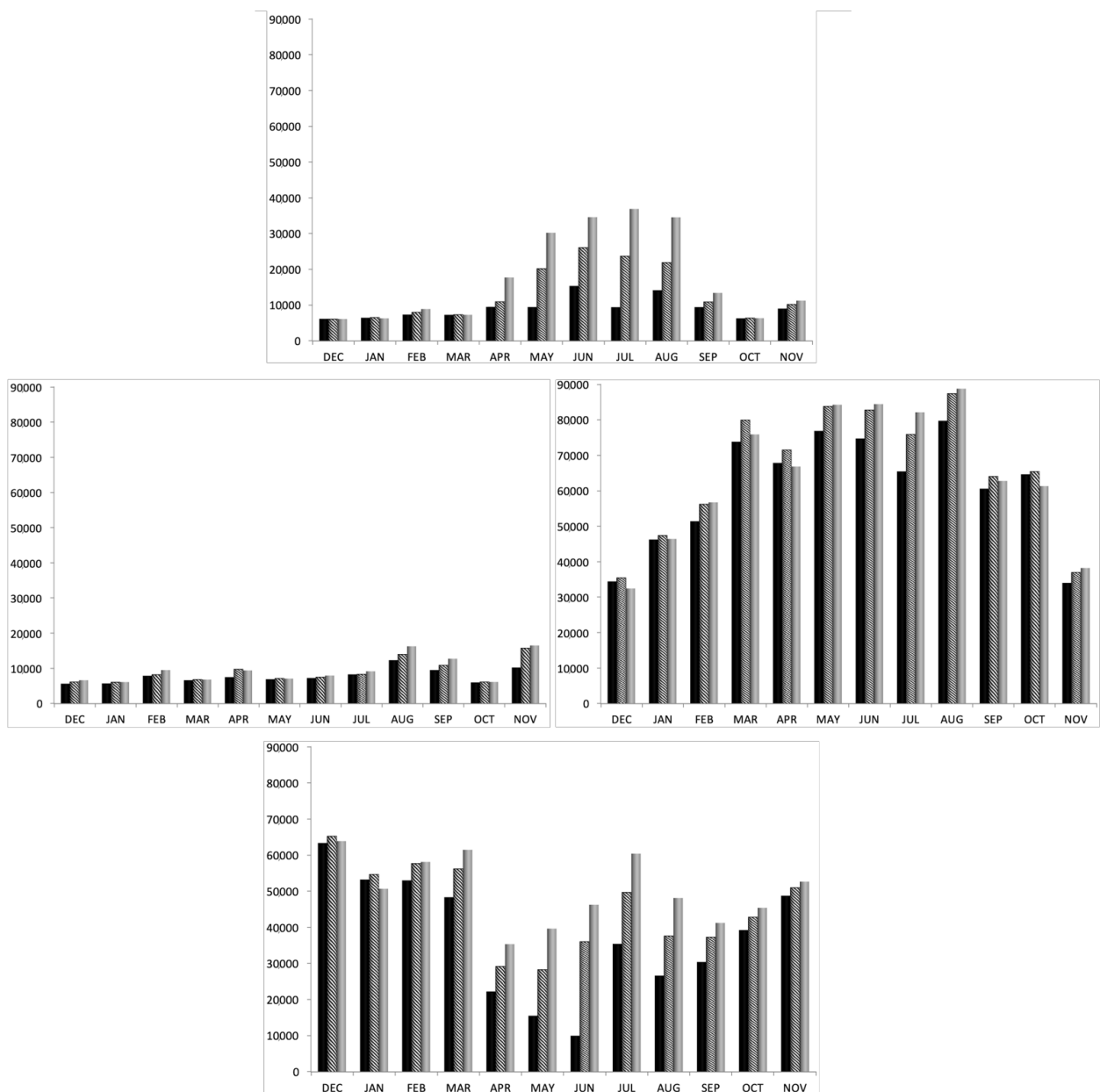


Figure 6. EDIs calculated depending on the season (from December 2018 to November 2019); orientation of north (**top**), east (**right**), south (**bottom**), and west (**left**); and elevation from the horizontal level of 15° (black), 30° (striped), and 45° (grey).

Both the photopic illuminances and EMLs reach higher illuminances in the east and south orientations and in the summer months, as is the case with the EDIs that can be calculated according to the relation $EML = 1.104 \text{ EDI}$. The minimum illuminances, both photopic and melanopic, were taken in December at a west orientation with an angle of 15°. The maximum illuminances, both photopic and melanopic, were taken in August at an east orientation with an angle of 45°, as has been previously described for EDI due to their proportionality relationship.

Bella et al. [17] modelled the nonvisual potential of daylight in terms of the melanopic/photopic ratio calculated from the SPD, finding values very close to 1 and similar to those calculated by using the D_{40} to D_{120} illuminances. Although this definition differs from our MAF, both indicate practically the same melanopic contribution as the photopic for daylight, and the spectra could be considered to be covering similar ranges to our CCTs.

Other authors have developed circadian theories. One of the most widespread is Rea et al. who defined the circadian stimulus (CS) and the CL_A , parameters directly proportional to the levels of night-time light-induced melatonin suppression [29]. This method is not based on any standard but has been adopted by most researchers to define the circadian effect of light [18]. The highest CS, 0.699, is found in the south and east orientations than in the north and east orientations, especially in the winter months (Figure 7). The lowest CS found is in the month of December facing the west at 15° with a value of 0.685. Given the outdoor SPDs with higher short wavelength contributions than longer ones, the corresponding CSs are always very close to the 0.7 saturation value in the studied period during the evaluated hours. Our calculation shows a CS (mean \pm standard deviation) of 0.695 ± 0.004 throughout the evaluated year for all orientations and elevations with a variation of $<1\%$. There are higher CL_A values in the east followed by the south orientation, and the lowest values are in the west followed by the north orientation (Figure 8). The measurements taken at 45° are generally the highest values compared to those measured at 30° and those measured at 15° , which have the lowest values. The highest values measured in the east occur in spring and summer (from March to August) at the three elevations, and the lowest occur in the west in winter (from December to March). Our calculations show a CL_A (mean \pm standard deviation) of $77,935 \pm 62,347$ circadian lux (range 11,665–215,042 circadian lux). It should be noted that our obtained values of CL_A for daylight are proportional to the EDIs, as shown by the analysed data, with $CL_A = (2.3 \pm 0.1)$ EDI. Therefore, based on this relationship and for cool daylight, CL_A , EDI and EML are parameters proportional to each other.

According to the mathematical model based on spectral sensitivity data proposed by Rea et al. [29], CL_A provides information on the SPD at the corneal level converted into circadian light [30,31]; and the CS, based on the CL_A , is equal to the percentage of melatonin suppression [32], ranging from threshold (CS = 0.1) to saturation (CS = 0.7) [33]. The CS seems to be necessary to promote circadian entrainment. As our mean CS obtained is 0.695 ± 0.004 with a variation of 1%, it could be considered sufficient for the described saturation. Therefore, CS could be used directly to quantify the circadian impact of lighting. The values calculated in our study show that there would be a high percentage of melatonin suppression independent of the seasonality, orientation and elevation. Studies show that a CS equal to or greater than 0.3 (equivalent to 30% melatonin suppression) in the first part of the day can improve the circadian cycle and the quality of sleep, reduce drowsiness and increase vitality and alertness [31,33–35], which coincides with our data collected from 10:00 to 11:00 AM.

A value of CS = 0.35 was proposed as a sufficient and adequate value to promote the daily cycle [36]. According to Rea, the daylight spectrum has been shown to be relatively efficient in providing circadian stimulation; and based on the CIE D_{65} spectrum, a corneal illuminance of 233 lx corresponds to this 0.35 CS. Extrapolating our outdoor analysis to indoor situations, circadian efficiency should be treated with caution because artificial lighting seems to be less effective since for the same value of CS = 0.35, a corneal illuminance much higher than that necessary with natural light would be needed [37]. All the outdoor SPDs collected for this paper are, regarding the CCT, above 4800 K, meaning that for indoor lighting purposes, it would be equivalent to cold light; and, assuming the same light intensity, higher CCT values indicate a greater perception of luminosity. This fact could improve visual performance and the relative effectiveness of light sources with higher melanopic intensity. This situation will be favourable for improving indoor performance in the morning hours; however, in the afternoon and at night, it will be more convenient to use warm lighting with low melanopic intensity [9,15]. In an investigation of a method to evaluate the nonvisual potential of daylight in two European cities, CCTs between 4631 K and 11,871 K were recorded in Naples and CCTs between 3585 K and 9812 K were recorded in Bialystock [17]. These results are similar to those of this study since our CCT measurements vary between 4892 and 12,380 K. However, due to the low correlation between the CCT and circadian effects, it is considered that the CCT is not a good indicator

to establish the levels of circadian response [20,37]. Although Rea et al. reported that LEDs with high CCTs above 5299 k could slightly stimulate the circadian system after one hour of exposure to outdoor lighting at 95 lux, when taking advantage of natural light in interior spaces, the reflectance of the walls must also be considered because they vary the CCT and the spectral composition of light that regulate the circadian system [38–40]. Additionally, our measurements show that for indoor purposes where daylight reaching outdoors is important, new parameters, such as the seasonality, façade orientation and altitude of the sun, are substantial and have sufficient contributions that should always be considered.

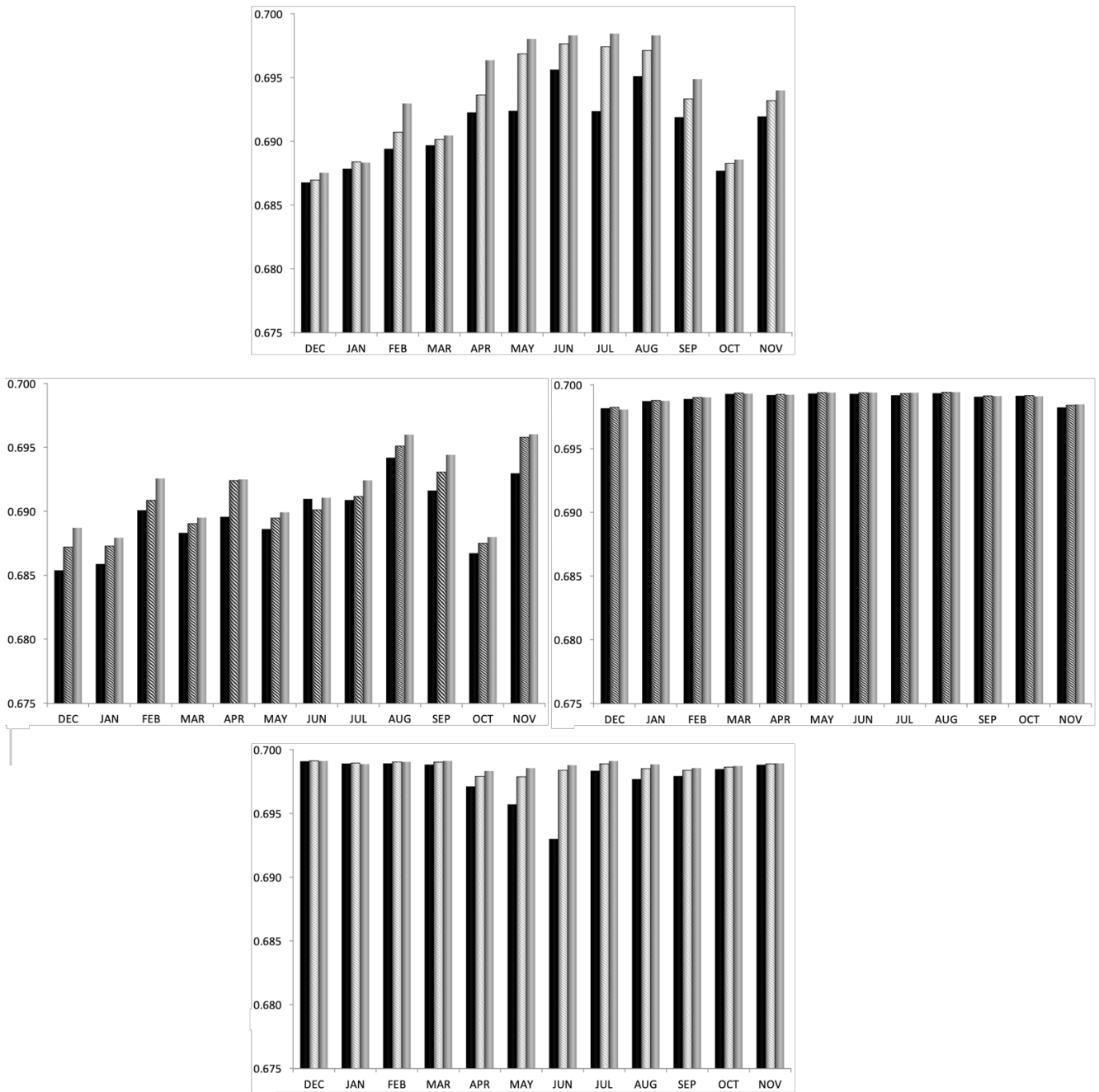


Figure 7. CS values calculated depending on the season (from December 2018 to November 2019); orientation of north (top), east (right), south (bottom), and west (left); and elevation from the horizontal level of 15° (black), 30° (striped), and 45° (grey).

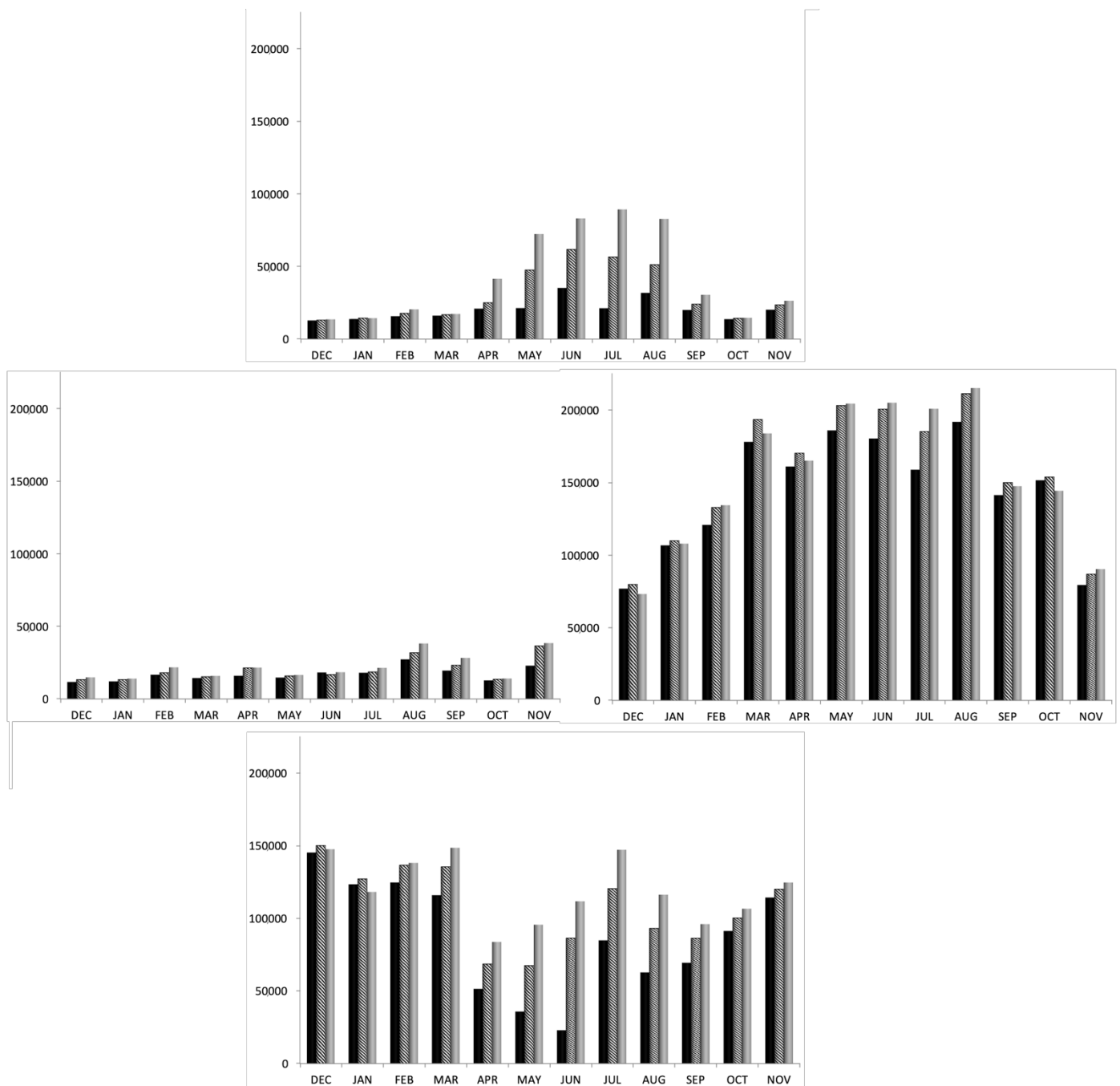


Figure 8. CL_A values calculated depending on the season (from December 2018 to November 2019); orientation of north (**top**), east (**right**), south (**bottom**), and west (**left**); and elevation from the horizontal level of 15° (black), 30° (striped), and 45° (grey).

4. Conclusions

The CIE Standard General Skies models the SPD of daylight according to the omnidirectional diffuse light reflected and refracted from the entire skydome and not just the highly directional rays from the sun. This standard makes it possible to derive coefficient values directly from measured instantaneous sky illuminance or irradiance or to adjust them independently to simulate and to match any sky conditions. Our benchmarking study reveals the differences in daylight SPDs, with the orientation, altitude and seasonality, on photopic and melanopic estimations, which could potentially modify occupants' responses in outdoor and indoor scenarios. Knowledge of the spectral and spatial patterns of daylight

is needed to develop simple outdoor circadian models and procedures to apply them, especially when they should be robust to indoor lighting projects. We have found that based on the CIE recommendations, intercomparison among metrics with high correlation has potential. In addition, the results presented in our study demonstrate that despite the significant variations in daylight SPD in a specific location, it is possible to evaluate the nonvisual potential of daylight based on the analysis of these spectra using the MAF parameter and traditional photopic illuminance.

In this study, the skies seasonality of Zaragoza during a year in terms of the SPD was studied. Selected clear skies have the highest contribution to both photopic and melanopic illuminances, but data relating to seasonality, sun altitude and glazing orientation in buildings have been measured. The results show that these factors should be considered when outdoor or indoor lighting projects are implemented.

As a limitation, further long-term SPD measurements are required for the annual study of a specific local daylight contribution. This could contribute to the establishment of general daylight indoor design rules based on real scenarios that consider the total information on the light that exists in the physical environment of each city. Information is lacking on how the daylight SPD may vary depending on geographic location and weather conditions; and another important aspect to consider is that due to the position of the sun vault in the skydome, the SPD is different on different vertical planes depending on both season and orientation. Having access to this information will allow the development of better guidelines not only for interior lighting design but also for the management and control of some biomedical questions such as dermatological [41,42] and psychiatric pathologies [43] or the improvement of some ocular dysfunctions in the fields of optometry and ophthalmology [44], among others. Finally, it was demonstrated that despite the dynamic variations in daylight and the corresponding variations in circadian values, for each orientation, altitude and season, it is possible to easily calculate a value describing the nonvisual potential of the daylight incidence at the building façade from photopic illuminance and knowing the SPD of the incident light.

Author Contributions: Conceptualization, J.A. and A.S.-C.; methodology, J.A. and A.S.-C.; validation, M.J.L. and I.P.; data curation, S.E. and E.O.-H.; writing—original draft preparation, S.E., E.O.-H. and A.S.-C.; writing—review and editing, J.A., E.O.-H. and A.S.-C. All authors have read and agreed to the published version of the manuscript.

Funding: This research was partially funded by the Spanish Agencia Estatal Investigación- European Fund for Regional Development, grant number PID2019-107058RB-I00.

Institutional Review Board Statement: Not applicable.

Informed Consent Statement: Not applicable.

Data Availability Statement: Not applicable.

Conflicts of Interest: The authors declare no conflict of interest.

References

1. ISO 15469: 2004. *Spatial Distribution of Daylight—CIE Standard General Sky*; CIE Central Bureau: Vienna, Austria, 2003.
2. Darula, S.; Kittler, R. A methodology for designing and calibrating an artificial sky to simulate ISO/CIE sky types with an artificial sun. *Leukos* **2015**, *11*, 93–105. [[CrossRef](#)]
3. Kim, C.; Kim, K. Development of sky luminance and daylight illuminance prediction methods for lighting energy saving in office buildings. *Energies* **2019**, *12*, 592. [[CrossRef](#)]
4. Perez, R.; Ineichen, P.; Seals, R.; Michalsky, J.; Stewart, R. Modeling daylight availability and irradiance components from direct and global irradiance. *Sol. Energy* **1990**, *44*, 271–289. [[CrossRef](#)]
5. Li, D.H.; Lou, S. Review of solar irradiance and daylight illuminance modeling and sky classification. *Renew. Energy* **2018**, *126*, 445–453. [[CrossRef](#)]
6. BS EN 12464-1:2011. *Light and Lighting—Lighting of Work Places—Part 1: Indoor Work Places*; BSI Standards Publication: London, UK, 2011.
7. UNE EN 12464-2:2016. *Light and Lighting—Lighting of Work Places—Part 2: Outdoor Work Places*; BSI Standards Publication: London, UK, 2011.

8. Wild, C.P. Complementing the genome with an “exposome”: The outstanding challenge of environmental exposure measurement in molecular epidemiology. *Cancer Epidemiol. Biomark. Prev.* **2005**, *14*, 1847–1850. [[CrossRef](#)]
9. Lucas, R.J.; Peirson, S.N.; Berson, D.M.; Brown, T.M.; Cooper, H.M.; Czeisler, C.A.; Figueiro, M.G.; Gamlin, P.D.; Lockley, S.W.; O’Hagan, J.B.; et al. Measuring and using light in the melanopsin age. *Trends Neurosci.* **2014**, *37*, 1–9. [[CrossRef](#)]
10. CIE S 026/E:2018. *CIE System for Metrology of Optical Radiation for ipRGC-Influenced Responses to Light*; CIE Central Bureau: Vienna, Austria, 2018.
11. Khademagha, P.; Aries, M.; Rosemann, A.; van Loenen, E.J. Implementing non-image-forming effects of light in the built environment: A review on what we need. *Build. Environ.* **2016**, *108*, 263–272. [[CrossRef](#)]
12. CIE. *Position Statement on Non-Visual Effects of Light—Recommending Proper Light at the Proper Time*, 2nd ed.; CIE Central Bureau: Vienna, Austria, 2019.
13. International WELL Building Institute (IWBI) WELL Building Standard. LIGHT. WELL v2. Q2 2021. Available online: <https://standard.wellcertified.com/well> (accessed on 12 May 2021).
14. Brown, T.; Brainard, G.; Cajochen, C.; Czeisler, C.; Hanifin, J.; Lockley, S.; Lucas, R.; Munch, M.; O’Hagan, J.; Peirson, S. Recommendations for healthy daytime, evening, and night-time indoor light exposure. *Preprints* **2020**. [[CrossRef](#)]
15. Schlangen, L.J.; Price, L.L. The Lighting environment, its metrology, and non-visual responses. *Front. Neurol.* **2021**, *12*, 235. [[CrossRef](#)]
16. Brainard, G.C.; Hanifin, J.P.; Greeson, J.M.; Byrne, B.; Glickman, G.; Gerner, E.; Rollag, M.D. Action spectrum for melatonin regulation in humans: Evidence for a novel circadian photoreceptor. *J. Neurosci.* **2001**, *21*, 6405–6412. [[CrossRef](#)]
17. Bellia, L.; Błaszczak, U.; Fragliasso, F.; Gryko, L. Matching CIE illuminants to measured spectral power distributions: A method to evaluate non-visual potential of daylight in two European cities. *Sol. Energy* **2020**, *208*, 830–858. [[CrossRef](#)]
18. Bellia, L.; Fragliasso, F. Good places to live and sleep well: A literature review about the role of architecture in determining non-visual effects of light. *Int. J. Environ. Res. Public Health* **2021**, *18*, 1002. [[CrossRef](#)]
19. Wyszecki, G.; Stiles, W.S. *Color Science*; Wiley: New York, NY, USA, 1982; Volume 8.
20. Sánchez-Cano, A.; Aporta, J. Optimization of lighting projects including photopic and circadian criteria: A simplified action protocol. *Appl. Sci.* **2020**, *10*, 8068. [[CrossRef](#)]
21. Gall, D.; Bieske, K. *Definition and Measurement of Circadian Radiometric Quantities*; Ilmenau University of Technology: Ilmenau, Germany, 2004.
22. Diakite, A.K.; Knoop, M. Data-driven spectral sky models: A review. *J. Int. Colour Assoc.* **2019**, *23*, 55–61.
23. Knoop, M.; Weber, N.; Diakite, A. Approach to analyse seasonal and geographical variations in daylight illuminants. In Proceedings of the CIE x046: 2019 Proceedings of the 29th CIE Session, Washington DC, USA, 14–22 June 2019.
24. Hernández-Andrés, J.; Romero, J.; Nieves, J.L.; Lee, R.L. Color and spectral analysis of daylight in southern Europe. *JOSA A* **2001**, *18*, 1325–1335. [[CrossRef](#)] [[PubMed](#)]
25. Spitschan, M.; Aguirre, G.K.; Brainard, D.H.; Sweeney, A.M. Variation of outdoor illumination as a function of solar elevation and light pollution. *Sci. Rep.* **2016**, *6*, 1–14.
26. Peyvandi, S.; Hernández-Andrés, J.; Olmo, F.J.; Nieves, J.L.; Romero, J. Colorimetric analysis of outdoor illumination across varieties of atmospheric conditions. *JOSA A* **2016**, *33*, 1049–1059. [[CrossRef](#)]
27. Condit, H.R.; Grum, F. Spectral energy distribution of daylight. *Josa* **1964**, *54*, 937–944. [[CrossRef](#)]
28. Li, D.H.; Chau, T.C.; Wan, K.K. A review of the CIE general sky classification approaches. *Renew. Sustain. Energy Rev.* **2014**, *31*, 563–574. [[CrossRef](#)]
29. Rea, M.S.; Figueiro, M.G.; Bierman, A.; Hamner, R. Modelling the spectral sensitivity of the human circadian system. *Light. Res. Technol.* **2012**, *44*, 386–396. [[CrossRef](#)]
30. Cai, W.; Yue, J.; Dai, Q.; Hao, L.; Lin, Y.; Shi, W.; Huang, Y.; Wei, M. The impact of room surface reflectance on corneal illuminance and rule-of-thumb equations for circadian lighting design. *Build. Environ.* **2018**, *141*, 288–297. [[CrossRef](#)]
31. Rea, M.S.; Figueiro, M.G. Light as a circadian stimulus for architectural lighting. *Light. Res. Technol.* **2018**, *50*, 497–510. [[CrossRef](#)]
32. Figueiro, M.G.; Kalsher, M.; Steverson, B.C.; Heerwagen, J.; Kampschroer, K.; Rea, M.S. Circadian-effective light and its impact on alertness in office workers. *Light. Res. Technol.* **2019**, *51*, 171–183. [[CrossRef](#)]
33. Figueiro, M.G.; Nagare, R.; Price, L. Non-visual effects of light: How to use light to promote circadian entrainment and elicit alertness. *Light. Res. Technol.* **2018**, *50*, 38–62. [[CrossRef](#)] [[PubMed](#)]
34. Figueiro, M.G.; Steverson, B.; Heerwagen, J.; Kampschroer, K.; Hunter, C.M.; Gonzales, K.; Plitnick, B.; Rea, M.S. The impact of daytime light exposures on sleep and mood in office workers. *Sleep Health* **2017**, *3*, 204–215. [[CrossRef](#)] [[PubMed](#)]
35. Acosta, I.; Leslie, R.P.; Figueiro, M.G. Analysis of circadian stimulus allowed by daylighting in hospital rooms. *Light. Res. Technol.* **2017**, *49*, 49–61. [[CrossRef](#)]
36. Dai, Q.; Huang, Y.; Hao, L.; Lin, Y.; Chen, K. Spatial and spectral illumination design for energy-efficient circadian lighting. *Build. Environ.* **2018**, *146*, 216–225. [[CrossRef](#)]
37. Li, M.; Wu, P.; Ding, J.; Yao, Q.; Ju, J. The circadian effect versus mesopic vision effect in road lighting applications. *Appl. Sci.* **2020**, *10*, 6975. [[CrossRef](#)]
38. Sánchez-Cano, A.; Pérez, O.L.; Aporta, J. Proposal to calculate the circadian component in lighting projects. *Opt. Pura. Apl.* **2019**, *52*, 1–11. [[CrossRef](#)]

39. Yao, Q.; Cai, W.; Li, M.; Hu, Z.; Xue, P.; Dai, Q. Efficient circadian daylighting: A proposed equation, experimental validation, and the consequent importance of room surface reflectance. *Energy Build.* **2020**, *210*, 109784. [[CrossRef](#)]
40. Parsaee, M.; Demers, C.M.; Lalonde, J.; Potvin, A.; Inanici, M.; Hébert, M. Human-centric lighting performance of shading panels in architecture: A benchmarking study with lab scale physical models under real skies. *Sol. Energy* **2020**, *204*, 354–368. [[CrossRef](#)]
41. O'Mahoney, P.; Khazova, M.; Higlett, M.; Lister, T.; Ibbotson, S.; Eadie, E. Use of illuminance as a guide to effective light delivery during daylight photodynamic therapy in the UK. *Br. J. Dermatol.* **2017**, *176*, 1607–1616. [[CrossRef](#)]
42. O'Mahoney, P.; Khazova, M.; Eadie, E.; Ibbotson, S. Measuring daylight: A review of dosimetry in daylight photodynamic therapy. *Pharmaceuticals* **2019**, *12*, 143. [[CrossRef](#)]
43. Münch, M.; Wirz-Justice, A.; Brown, S.A.; Kantermann, T.; Martiny, K.; Stefani, O.; Vetter, C.; Wright, K.P., Jr.; Wulff, K.; Skene, D.J. The role of daylight for humans: Gaps in current knowledge. *Clocks Sleep* **2020**, *2*, 8. [[CrossRef](#)]
44. Troilo, D.; Smith, E.L.; Nickla, D.L.; Ashby, R.; Tkatchenko, A.V.; Ostrin, L.A.; Gawne, T.J.; Pardue, M.T.; Summers, J.A.; Kee, C. IMI–Report on experimental models of emmetropization and myopia. *Investig. Ophthalmol. Vis. Sci.* **2019**, *60*, M31–M88. [[CrossRef](#)] [[PubMed](#)]